Forward Modeling of the Phobos Tides and applications to the InSight mission

L. Pou[a], F. Nimmo[a], P. Lognonné[b], D. Mimoun[c], R. F. Garcia[c], A. Rivoldini[d], D. Banfield[e], W. B. Banerdt[f]

[a]*Dept. Earth and Planetary Sciences, University of California Santa Cruz*, **Santa Cruz, USA** ***(lpou@ucsc.edu)*** [b]Institut de Physique du Globe de Paris, *Paris, France* [c]DEOS/SSPA *Institut Supérieur de l'Aéronautique et de l'Espace, Toulouse, France* [d]Royal Observatory of Belgium, *Brussels, Belgium* [e]Cornell University, *Ithaca, USA* [f]Jet Propulsion Laboratory, *Pasadena, USA*

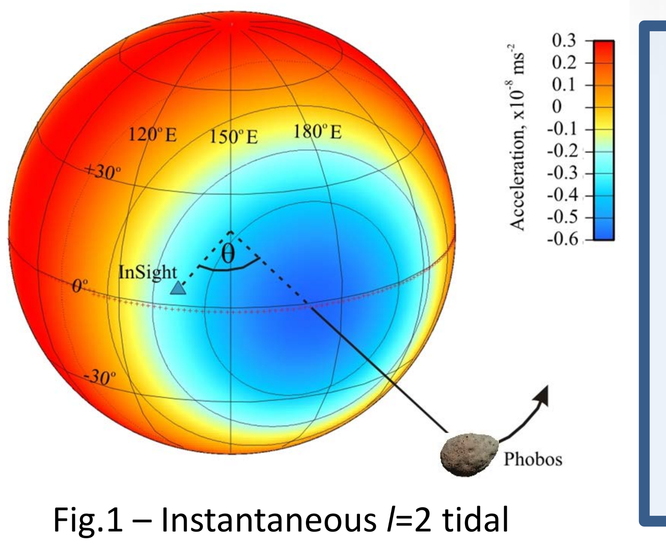

Fig.1 – Instantaneous *l*=2 tidal acceleration from Phobos.

By using the VBB seismometer of SEIS as a gravimeter on the surface of Mars, the InSight mission will provide long-period data suited to tidal analysis [1,2]. **The tidal response of Mars**, due to the Sun and the Martian moons, Phobos and Deimos, provides **information about the interior structure of Mars**. Most notably, **the proximity of Phobos means that degree-2, -3 -4 and further tides are all detectable** and will be sensitive to the rheology of different depth ranges within Mars [3] (Fig. 1). While less than 8% of the main Solar tide amplitude, **the Phobos tides** occupy a range of frequencies separate from the diurnal harmonics, **making their recovery easier** [4] (Fig. 2).

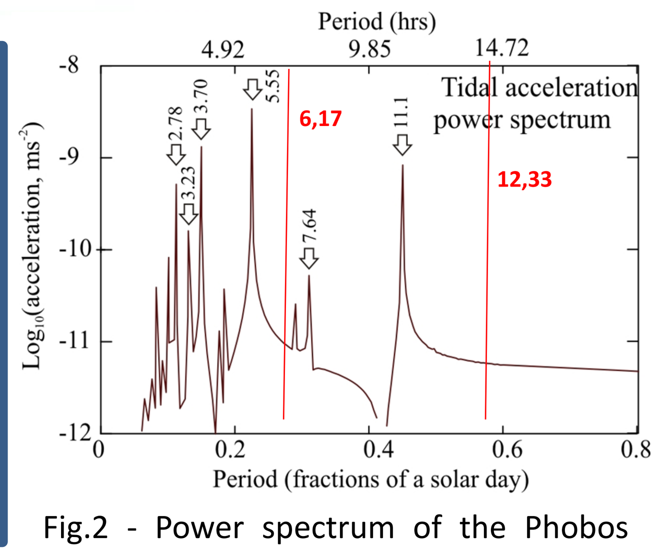

Fig.2 - Power spectrum of the Phobos tides acceleration. Individual peaks are marked with period in hours. Main solar tides are indicated with vertical red lines.

Forward modeling of the tides

We build a **forward model of the expected acceleration** recorded by InSight due to the **Phobos tides** using **ephemerides from the JPL Horizons website** to take into account all the physical parameters of Phobos' orbit, such as eccentricity, inclination, obliquity and apsidal precession. From the position of Phobos in the Martian sky, its ground track is derived and **the tidal potential of Phobos is calculated for degree l=2, 3 and 4** (Fig. 3).

The magnitude of the change in gravity due to the Phobos tides depends on the **gravimetric factor** δ_l [3]:

$$\Delta g_l = -\delta_l \left[g_0 l \frac{m_p}{M_m} \left(\frac{R}{r}\right)^{l+1} \right]$$

with m_p, M_m the mass of Phobos and Mars, R the Martian radius and r the distance between them.

Between the actual position of Phobos and the change in local gravity, there will also be a **phase lag** ϵ due to the difference of rotation between the Martian surface, the rotational speed of the Martian moon and the dissipation inside Mars [6]:

$$\epsilon_{lm} = \frac{1}{Q_l} = m\, \alpha_{lm}$$

with m being the order of the considered tide, and α_{lm} the geometric lag angle between Phobos and the tidal bulge induced by Phobos (Fig. 4).

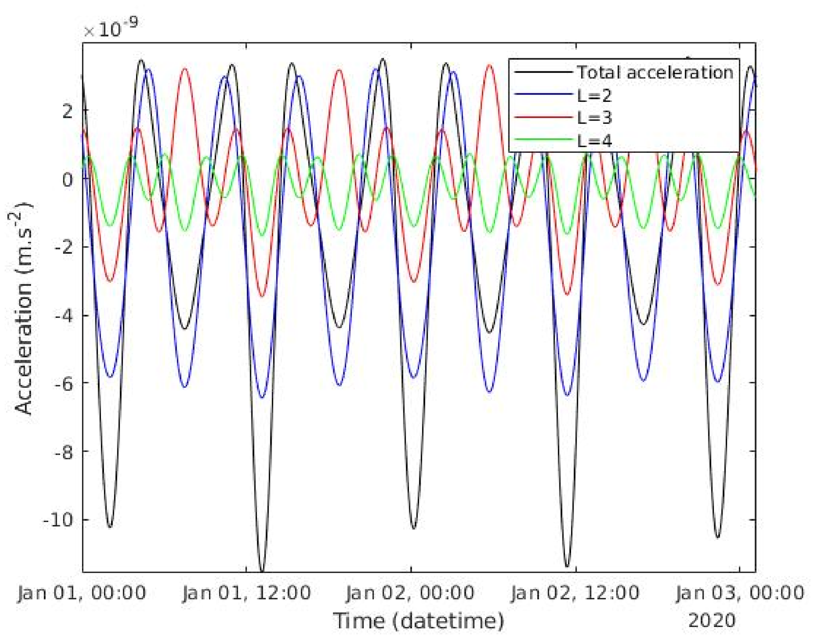

Fig.3 – Tidal potential of Phobos derived from the JPL Horizons website, calculated for degree 2, 3 and 4. Main Phobos tide has a period of 5h33min.

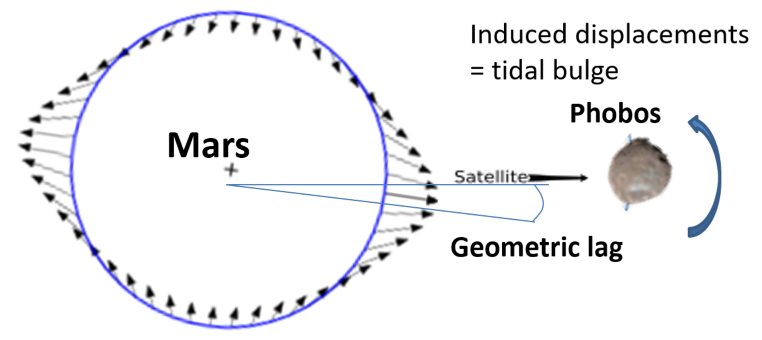

Fig.4 – Phobos creates a tidal bulge at the surface of Mars; however, since it rotates faster than the surface of Mars, there is a geometric lag angle between its actual position and the Phobos tides induced displacements.

Signals seen by SEIS

Besides the gravity variations due to the Phobos tides, SEIS is also sensitive to other signals, here seen as noise sources. Among those, the strongest contributors are the **thermal noise** and the **pressure noise**, with respective amplitudes $8x\,10^{-4}$ and $4x\,10^{-6}\, m.s^{-2}$ at the diurnal frequency [4], compared with the full tidal signal of $6x\,10^{-9}\, m.s^{-2}$ at the l=2 Phobos tide frequency. This results in a **signal-to-noise ratio** around $\mathbf{10^{-5}}$ [4] and therefore a combination of noise removal and filtering is needed.

For this work, the same **noise models from Pou et al. (2019) [4] and Mimoun et al. (2017) [7]** are used but **updated with the actual temperature and pressure measurements from InSight** for the long period noises. The difference between the updated models and the expected noises from [4] are shown in Fig. 5 and compared with the expected tidal signal amplitudes, showing **good agreement with the previous works** of [4]; thus, **we are using the same method to recover the Phobos tides.**

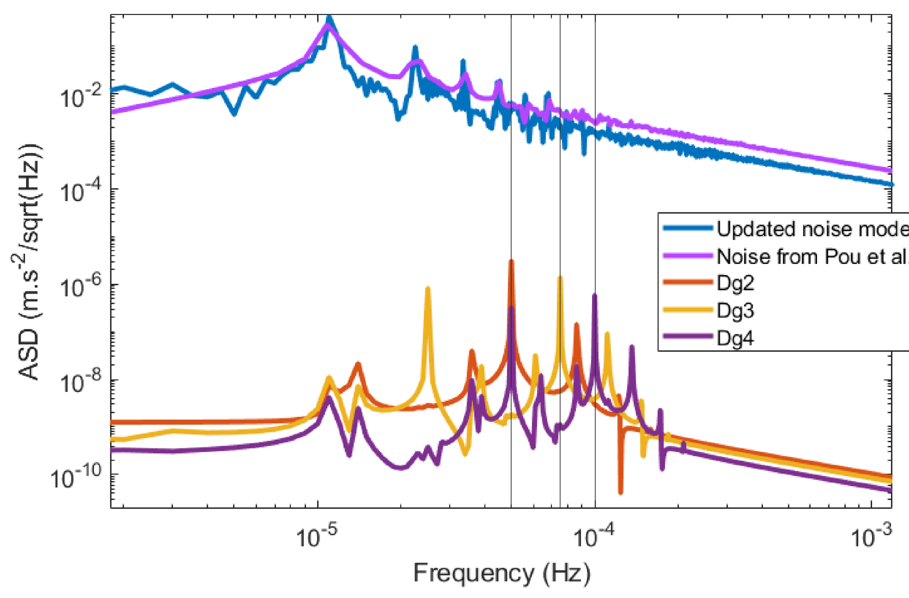

Fig.5 – Expected SEIS output on the vertical axis (blue – this work, pink from [4]) compared to the expected gravity variations due to the tides of degree 2 (Dg2, orange), degree 3 (Dg3, yellow), and degree 4 (Dg4, purple). The main frequencies of the tides are indicated by black lines.

Martian interior models

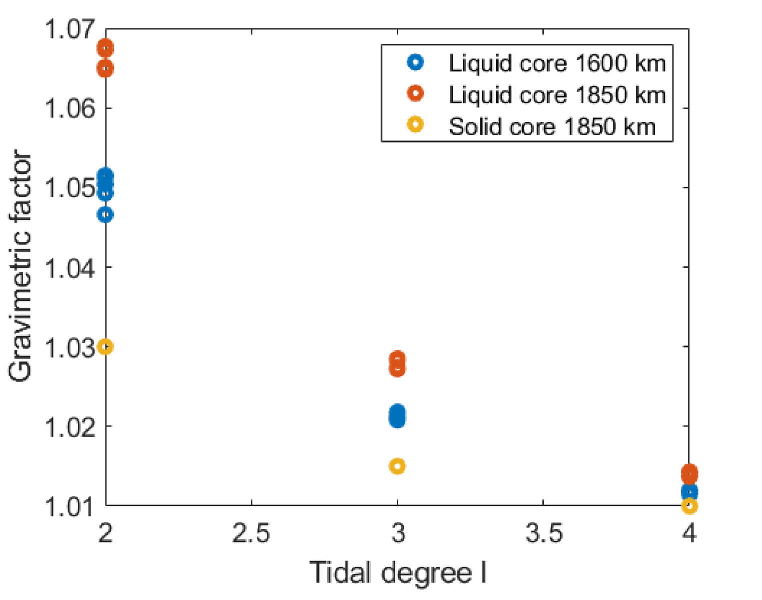

Fig. 6 – Gravimetric factors for various Martian models and tidal degrees, illustrating the impact of the state and size of the core on the gravity variations at the surface of Mars. For each model, Q_2 = 80 or 105, but it has nearly no impact on the gravimetric factor.

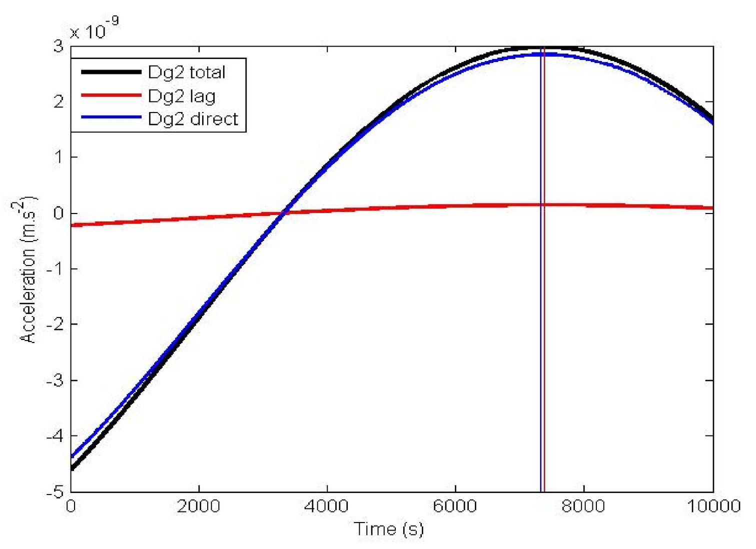

Fig. 7 – Acceleration due to the degree-2 Phobos tide. The blue component is due to the direct attraction of Phobos, and the red due to the tidal displacements of Mars creating a change in the local gravity, affected by the geometric lag angle.

Several Martian models have been considered to calculate the **expected magnitude of the gravity variations and phase lags**.

The first set of models are based on the mantle composition of Taylor et al. (2007) [8], the rheology model of Faul and Jackson (2007) [9] and the hot temperature end-member of Plesa et al. (2015) [10]. The core is assumed to be made of liquid Fe-S core and based of the thermoplastic data of Terasaki et al. (2019) [11]. The **second set of models** is based on the mantle composition from Yoshizaki and McDonough (2019) [12] and uses either the hot temperature end-member or a profile in-between the hot and cold end-member of Plesa et al. (2015) [10]. The **last model** is made with a solid core based on Nimmo and Faul (2013) [13].

From these models we compute the **Love numbers h and k** for degree l=2, 3 and 4, as well as the associated **gravimetric factors** as [6]:

$$\delta_l = 1 - \frac{l+1}{l} k_l + \frac{2}{l} h_l$$

This gives us a **range of various gravimetric factors and phase lags** (Fig. 6) to model the actual acceleration due to the Phobos tides at the surface of Mars in both amplitude and phase (as in Fig. 7 for the degree-2 tides).

Results

The gravimetric factors for the different Mars models are given in Fig. 6. Using this figure, we can deduce the accuracy needed on the recovery of the Phobos tides to constrain the Martian interior (Table 1). **Here, data are simulated over 2 Earth years** (nominal duration of the InSight mission).

Assuming an error of 0.4% on the VBB gain, the tidal signals extraction error and by including the errors on the Phobos ephemerides, the **absolute gravimetric factors** can be retrieved at **1.1% for δ_2, 1.4% for δ_3 and 1.0% for δ_4** (Fig. 8) due to uncertainties.

In order to **reduce the errors** notably in the Phobos ephemerides (0.5%) and in the knowledge of the absolute gain of SEIS (at best 0.4%), a better way can be to recover **the relative gravimetric factor ratio** [5]. This way, our recovery method on δ_3/δ_2 **is about 1.5%, and δ_4/δ_2 is recovered with an error of 1.1%.**

Therefore, by estimating the gravimetric factors, **it should be possible after 2 Earth years to constrain the state of the core and its size to at least ± 125 km.**

Parameter	Accuracy needed for state of core	Accuracy needed for size ± 125 km	Parameter recovery
δ_2	3.4%	1.2%	1.1%
δ_3	1.2%	0.5%	1.4%
δ_4	0.4%	0.2%	1.0%
δ_3/δ_2	2%	0.8%	1.5%
δ_4/δ_2	2.2%	1.2%	1.1%

from the models shown in Fig. 6, and current recovery values on synthetic data.

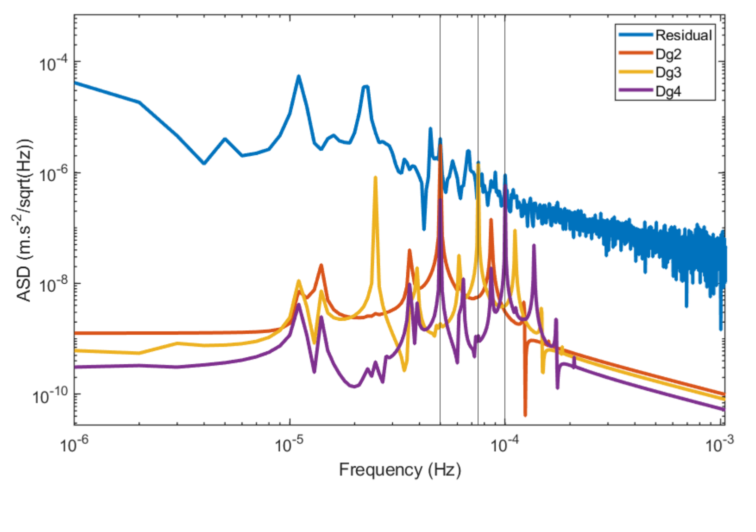

Fig. 8 – Result of the tides recovery algorithm described in [4] on synthetic data. The Phobos tides of degree-2, 3 and 4 are visible in the spectrum of the residual after matched filters and LMS filtering. The main frequencies of the tides are indicated by black lines.

Acknowledgments: This study is supported in part by the NASA InSight participating scientist program (NNH17ZDA001N-INSTPSP).

References : [1] Lognonné, P and Mosser, B. (1993) Surv. Geophys., 14, 239-302. [2] Lognonné, P. et al. (1996) Planet. Space. Sci., 44, 1237-1249. [3] Van Hoolst, T. et al. (2003) Icarus 161 281-296. [4] Pou, L. et al. (2019) (2019) Space Sci. Rev. 215: 6. [5] Lognonné, P. et al (2019) Space Sci. Rev. 2015:12. [6] Taylor, P.A. and Margot, J.L. (2010) Celest Mech Dyn Astr, 108: 315. [7] Mimoun, D. et al. (2017) Space Sci. Rev. 211: 383. [8] Taylor, G.J. et al. (2007) J. Geophys. Res., 111, E03S10. [9] Faul, U.H. and Jackson, I. (2007) J. Geophys. Res., 112, B04204. [10] Plesa, A.-C. et al. (2015) J. Geophys. Res. Planets, 120, 995-1010. [11] Terasaki, H. et al. (2019) J. Geophys. Res. Planets, 124, 2272-2293 [12] Yoshizaki, T. and McDonough, W.F. (2019) arXiv:1909.07560 [13] Nimmo, F and Faul, U. H. (2013) J. Geophys. Res. Planets, 118, 2558–2569.